Origins and Scaling of Hot-Electron Preheat in Ignition-Scale Direct-Drive Inertial Confinement Fusion Experiments

M. J. Rosenberg,[1,*] A. A. Solodov,[1] J. F. Myatt,[1,†] W. Seka,[1] P. Michel,[2] M. Hohenberger,[2] R. W. Short,[1] R. Epstein,[1] S. P. Regan,[1] E. M. Campbell,[1] T. Chapman,[2] C. Goyon,[2] J. E. Ralph,[2] M. A. Barrios,[2] J. D. Moody,[2] and J. W. Bates[3]
[1]*Laboratory for Laser Energetics, University of Rochester, Rochester, New York 14623, USA*
[2]*Lawrence Livermore National Laboratory, Livermore, California 94550, USA*
[3]*U. S. Naval Research Laboratory, Washington, DC 20375, USA*

(Received 18 July 2017; revised manuscript received 18 October 2017; published 29 January 2018)

Planar laser-plasma interaction (LPI) experiments at the National Ignition Facility (NIF) have allowed access for the first time to regimes of electron density scale length (~500 to 700 μm), electron temperature (~3 to 5 keV), and laser intensity (6 to 16×10^{14} W/cm^2) that are relevant to direct-drive inertial confinement fusion ignition. Unlike in shorter-scale-length plasmas on OMEGA, scattered-light data on the NIF show that the near-quarter-critical LPI physics is dominated by stimulated Raman scattering (SRS) rather than by two-plasmon decay (TPD). This difference in regime is explained based on absolute SRS and TPD threshold considerations. SRS sidescatter tangential to density contours and other SRS mechanisms are observed. The fraction of laser energy converted to hot electrons is ~0.7% to 2.9%, consistent with observed levels of SRS. The intensity threshold for hot-electron production is assessed, and the use of a Si ablator slightly increases this threshold from $\sim 4 \times 10^{14}$ to $\sim 6 \times 10^{14}$ W/cm^2. These results have significant implications for mitigation of LPI hot-electron preheat in direct-drive ignition designs.

DOI: 10.1103/PhysRevLett.120.055001

Direct-drive laser inertial confinement fusion (ICF) [1,2] is one of two laser-based techniques being pursued for achieving controlled nuclear fusion at the 1.8-MJ National Ignition Facility (NIF) [3]. In direct-drive hot-spot ignition designs, laser ablation of a spherical shell drives the implosion and compression of a cryogenic deuterium-tritium (DT) fuel layer, into which a fusion burn wave propagates after being initiated in a central, low-density hot spot [4]. To achieve ignition, the fuel must be compressed to an areal density greater than 0.3 g/cm^2, which can be achieved by keeping the pressure close to the Fermi-degenerate pressure. Preheat by suprathermal electrons generated by laser-plasma instabilities (LPI) increases this pressure, degrades compression, and inhibits ignition. Consequently, control of LPI suprathermal (or "hot")-electron production is critical for a successful implosion.

Stimulated Raman scattering (SRS) [5–8] and two-plasmon decay (TPD) [9] are two instabilities capable of generating hot electrons since they both excite electrostatic plasma waves that provide accelerating fields. SRS entails the decay of a laser light wave into an electron plasma wave and a scattered light wave at densities at or below one-quarter of the critical density of the laser, while TPD is the decay of a laser light wave into two electrostatic plasma waves near the quarter-critical density. Previous studies of SRS and TPD have examined single-beam thresholds [9,10], quantified suprathermal electron production [6,11,12], explored collective multibeam processes [13–18], and investigated the source angular distribution of the resulting hot electrons [19]—an important consideration when computing preheat. SRS imposes serious constraints on ignition designs in the indirect-drive approach to ICF because of high single-beam intensities and large volumes of quasihomogeneous plasma in gas-filled hohlraums [20]. To date, direct-drive experiments have shown minimal SRS resulting from lower single-beam intensities and density scale lengths shorter than ignition scale.

The low level or absence of observable SRS in subscale (density scale length $L_n \sim 150$ μm and electron temperature $T_e \sim 2$ keV) direct-drive implosions on the OMEGA laser [21] has focused work instead on the physics, scaling, and mitigation of TPD, which is observed close to threshold [15]. Direct-drive implosions on OMEGA are known to excite collective multibeam TPD, which, at the highest-available irradiation intensities, converts as much as 1% of the incident laser energy to hot electrons. This level of hot electrons, depending on their transport, is close to what can be tolerated in direct-drive ignition designs, and the scaling of hot electron production to ignition scale has not yet been assessed. Ignition-scale direct-drive implosions [22] will have much longer density scale lengths ($L_n \sim 600$ μm) and hotter coronal electron temperatures ($T_e \lesssim 5$ keV), placing the interaction conditions in a previously unexplored regime. Until the experiments described herein, on a MJ-scale facility, it was not possible to simultaneously achieve the density scale length, laser intensity, electron

temperature, and transverse plasma dimensions that are characteristic of ignition-scale direct-drive implosions.

This Letter presents the first exploration of the LPI origins, scaling, and possible mitigation of hot electrons under direct-drive ignition-relevant conditions. These new observations indicate the dominance of SRS over TPD, a result not previously observed in direct-drive-relevant plasmas, with significant implications for ignition designs.

Planar targets were irradiated from one side with 351-nm laser light using a subset of NIF's 192 beams, with one-dimensional smoothing by spectral dispersion [23] at 90 GHz. These beams are arranged into cones that share a common angle with respect to the polar axis. The "inner" cones have angles of 23.5° and 30° (32 beams in each hemisphere), while the "outer" cones have angles of 44.5° and 50° (64 beams in each hemisphere). All targets described here—CH (or Si) disks with a diameter of 4.4 mm and a thickness of 1.2 mm (or 0.75 mm)—were irradiated from the southern hemisphere. Planar targets were chosen because they are the only way, currently, to achieve direct-drive ignition-relevant plasma conditions, while using a reduced laser energy (~200 kJ) on NIF. The use of planar targets also reduces the level of cross-beam energy transfer [24] relative to spherical targets, which allows for higher laser intensities at quarter critical and improves confidence in experiment modeling, although some stimulated Brillouin scattering is observed.

Time-resolved SRS diagnostics were located at polar angles of 23.5°, 30°, and 50° [25], as shown in Fig. 1. The targets were irradiated with laser pulses of duration ≤ 8 ns at vacuum overlapped intensities of $\leq 3 \times 10^{15}$ W/cm^2. The plasma evolution was simulated using the 2D radiation-hydrodynamics code DRACO [26] for comparison with experimental observations. The DRACO predictions for the density scale lengths and electron temperatures, in the quarter-critical density region $n_e = n_c/4$ (where n_e is the electron density and n_c is the critical density for the laser wavelength λ_0 (in μm), with $n_c \approx 1.1 \times 10^{21} \lambda_0^{-2}$ cm^{-3}), were $L_n \sim 500$ to 700 μm and $T_e \sim 3$ to 5 keV, respectively. DRACO simulations calculate that collisional absorption attenuates the laser intensity by ~50% on reaching the quarter-critical surface.

A time-resolved scattered-light spectrum obtained from NIF shot N160420-003 is shown in Fig. 1(a). It displays a narrow, intense feature at a wavelength slightly above 702 nm ($2\lambda_0$). A local (i.e., near $n_c/4$) electron temperature measurement can be obtained from this feature from the relation $T_{e,\mathrm{keV}} = \Delta\lambda_{\mathrm{nm}}/3.09$ [27], where $\Delta\lambda$ is the shift of the spectral peak from $2\lambda_0$ after applying corrections for Doppler and Dewandre shifts [28], with small uncertainties in these modeling-based corrections relative to measurement uncertainties [29]. The electron temperature inferred from this technique is $T_e = 4.5 \pm 0.2$ keV between $t = 5$ and 7 ns, with the uncertainty determined by the spectrometer calibration. The DRACO calculations predict a consistent temperature (4.5 keV), giving confidence in the numerical modeling of the corona and indicating that ignition-relevant temperatures have been achieved. Because of refraction effects, this spectral feature is emitted only parallel to the density gradient [30], and its observation required the target to be tilted 23° to face the diagnostic [Fig. 1(d)].

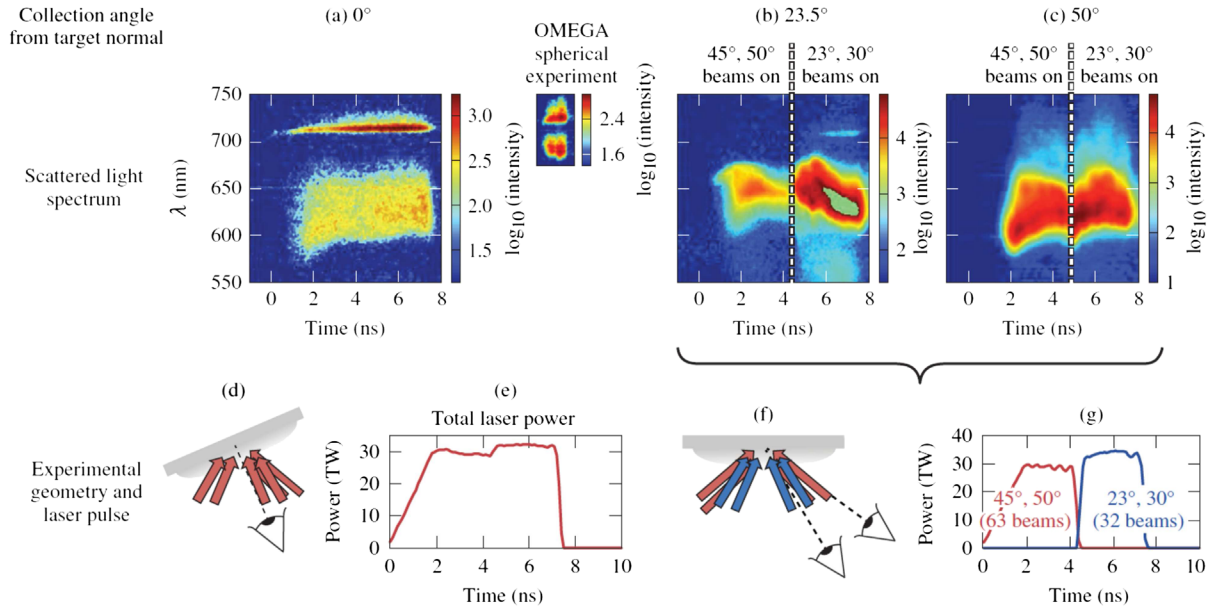

FIG. 1. Time-resolved scattered-light spectra at collection angles of (a) 0°, (b) 23.5°, and (c) 50° relative to the target normal. These images were obtained in two CH target experiments. The image in (a) corresponds to an experiment (d) with the target oriented toward a streaked spectrometer and (e) irradiated by a ramp-flat pulse. The images in (b) and (c) correspond to an experiment (f) with the target oriented toward the south pole of NIF and (g) irradiated first by beams at incidence angles of 45° and 50°, followed by beams at 23° and 30°. The streaked spectrum from a spherical-geometry experiment on OMEGA [inset in (a), same wavelength and time axes] is contrasted to the image in (a).

Importantly, this feature demonstrates significant differences relative to the near-$2\lambda_0$ spectrum obtained at smaller scales on OMEGA. A typical half-harmonic spectrum from a spherical implosion (shot 80802) on OMEGA is shown in the inset of Fig. 1(a). The characteristic half-harmonic features redshifted and blueshifted with respect to $2\lambda_0$ seen in the OMEGA experiment are a definitive diagnostic of the presence of TPD [27,31]. The lack of a blueshifted half-harmonic and the narrowness of the redshifted feature observed on NIF is a strong indication that different physical processes are occurring at the quarter-critical surface. The sharp feature observed in the NIF experiment is a well-known signature of the absolute Raman instability that can occur at densities around $n_c/4$ [27]. The OMEGA spectrum implies the absence of SRS around $n_c/4$ and the presence of TPD, while the NIF spectrum implies the presence of SRS at and below $n_c/4$. Although the presence of some TPD activity in the NIF experiment cannot be entirely ruled out on the basis of Fig. 1(a), since the conversion efficiencies of TPD waves to half-harmonic emission are difficult to quantify, it seems most plausible that SRS, rather than TPD, is the dominant quarter-critical LPI mechanism in ignition-scale direct-drive experiments.

Simple considerations based on the absolute threshold intensities for SRS ($I_{14}^{\mathrm{SRS,thr}} = 2377/L_{n,\mu\mathrm{m}}^{4/3}$) and TPD ($I_{14}^{\mathrm{TPD,thr}} = 233\ T_{e,\mathrm{keV}}/L_{n,\mu\mathrm{m}}$), for normally incident single plane-wave beams [9,10] qualitatively explain these observations. In these expressions, I_{14}^{thr} is the threshold intensity in units of 10^{14} W/cm^2. To illustrate, Fig. 2 shows the ratio of the absolute TPD threshold to the absolute SRS threshold as a function of electron temperature and density scale length. The OMEGA experiment that produced the TPD-dominated spectrum shown adjacent to Fig. 1(a) ($L_n \sim 150\ \mu$m, $T_e \sim 2.5$ keV, $I \sim 6 \times 10^{14}$ W/cm^2) appears marginally unstable with respect to TPD and slightly less stable to SRS if the total overlapped laser intensities are substituted

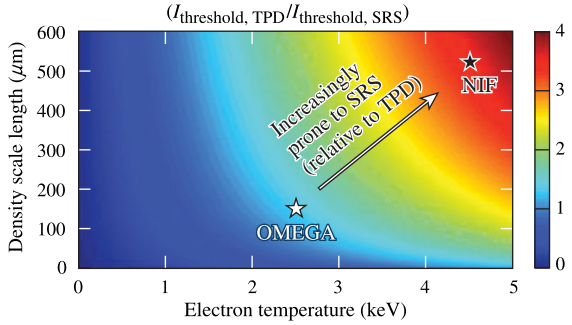

FIG. 2. Ratio of the absolute, single-beam intensity threshold for TPD [10] to the absolute, single-beam threshold for SRS [9] as a function of electron temperature and density scale length. Conditions corresponding to the NIF (OMEGA) spectra in Fig. 1(a) are represented by the black (white) star. With increasing scale length and temperature, SRS becomes increasingly prevalent with respect to TPD.

into the expressions for the single-beam thresholds. In contrast, the NIF experiment at ignition-relevant conditions ($L_n \sim 525\ \mu$m, $T_e \sim 4.5$ keV, $I \sim 1.3 \times 10^{15}$ W/cm^2), which produced the SRS-dominated spectrum shown in Fig. 1(a), is in a regime where the SRS threshold is several times less than the TPD threshold. As a caveat, this analysis does not account for potential differences in multibeam effects, which are known to be present for TPD on OMEGA [14], but is a subject of ongoing work for SRS on NIF. It is expected that this trend of SRS being increasingly prominent relative to TPD with increasing scale length and temperature [32] applies also for more-complicated cases of multiple obliquely incident beams.

The broad spectral features seen in Figs. 1(a)–1(c) are characteristic of SRS occurring at densities below $n_c/4$ (between 0.15 and 0.22 n_c). Figure 1(a) shows SRS along the target normal that is not due to single-beam backscatter; this is known because the beams along the diagnostic view were on only after 4.5 ns [corresponding to an increase in laser power as shown in Fig. 1(e)], and little difference in the SRS emission is observed. Figures 1(b) and 1(c) highlight SRS spectra obtained at two different angles of observation and two distinct irradiation conditions. The target normal was parallel to the NIF polar axis [Fig. 1(f)] and the target was irradiated symmetrically, first by outer beams from $t = 0$ to $t = 4.5$ ns, followed by inner beams from $t = 4.5$ to $t = 7.5$ ns [Fig. 1(g)]. The predicted quarter-critical plasma conditions during the outer (inner) beam drive were $L_n \sim 500\,(690)\ \mu$m, $I \sim 1.6\,(1.1) \times 10^{15}$ W/cm^2, and $T_e \sim 4.7\,(4.4)$ keV, respectively. Temporally resolved scattered-light spectra [25] were obtained at 23.5° [Fig. 1(b)] and 50° [Fig. 1(c)]. SRS is observed by both diagnostics at early times during outer beam irradiation and at later times when irradiated by inner beams.

These observations are attributed to several SRS mechanisms. The SRS observed at 23.5° [Fig. 1(b)] during the outer-beam drive is attributed to near-backscatter refracted closer to the target normal direction. During inner-beam drive, the SRS at 23.5° may be due to near-backscatter, sidescatter from other beams, or multiple-beam processes. SRS observed at 50° is attributed to sidescatter [18,33], with light waves propagating approximately tangentially to contours of constant electron density. The data shown in Fig. 1(c) cannot be explained by narrow angle backscatter, on account of refraction. For tangential sidescatter, the vacuum propagation direction (and collection angle) of SRS light, after refraction, is determined solely by its wavelength and depends only weakly on the incidence angle of the beams that produced it. This is evident in Fig. 1(c), where SRS light is observed at the same wavelength, ~620 nm, during both outer beam and inner beam irradiation. As tangential sidescatter growth is limited primarily by refraction of scattered light waves, it may be prevalent in spherical geometry as well.

To determine the total amount of SRS generated in these experiments, absolutely calibrated photodiodes measured

the SRS light collected in $\sim 2 \times 10^{-3}$ sr in two full aperture backscatter stations (FABSs) [25] at 50° and 30°. These measurements were then extrapolated to account for the total emission, using a ray-tracing code with plasma parameters and geometry provided by DRACO simulations to obtain simulated SRS emission profiles that include refraction and absorption as functions of wavelength and angle of observation (transmission of SRS light from its origin ranges from 2% at 702 nm to ~50% at 630 nm). These calculations assume 2π azimuthal symmetry around the target normal. It is estimated that between 2% and 6% of incident laser energy is converted to SRS light.

The inferred SRS light energy is compared to the energy in hot electrons, which is inferred from hard-x-ray bremsstrahlung emission generated by hot electrons interacting with the target [34]. This bremsstrahlung emission was detected using the NIF filter fluorescer (FFLEX) diagnostic [35]. The FFLEX signals were analyzed by performing Monte Carlo electron-photon transport calculations with the EGSnrc code [36], using a single-temperature ($T_{\rm hot}$) 3D Maxwellian hot-electron distribution. These calculations relate the absolute intensity of hard-x-ray emission to the total quantity of hot electrons. Figure 3 shows the corresponding fraction of laser energy converted to hot electrons ($f_{\rm hot}$) as a function of the DRACO-calculated laser intensity at the quarter-critical density for experiments using either CH or Si targets. The hard-x-ray data were integrated over the period of the experiment starting after 4.5 ns. For outer beam irradiation, $f_{\rm hot}$ increased from $0.7 \pm 0.2\%$ to $2.9 \pm 0.6\%$ as the laser intensity increased from 5.9×10^{14} to 14×10^{14} W/cm^2. For inner beam irradiation of CH targets, $f_{\rm hot}$ increased from $1.2 \pm 0.2\%$ to $2.6 \pm 0.5\%$ for intensities of 6.2×10^{14} to 11×10^{14} W/cm^2. For CH experiments, $T_{\rm hot}$ is inferred to be between 45 and 55 keV for the outer-beam drive and 62 keV for the inner-beam drive, independent of laser intensity, with an uncertainty of ±4 to

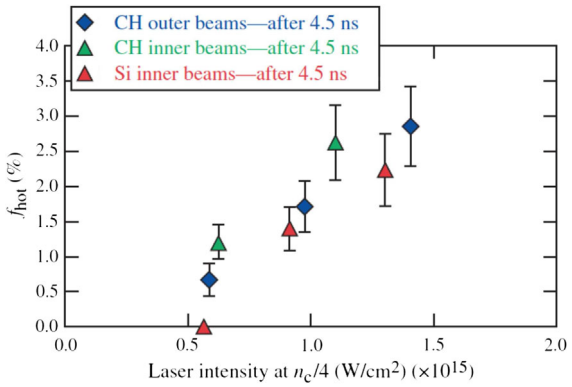

FIG. 3. Fraction of laser energy converted to hot electrons as a function of simulated quarter-critical laser intensity, for laser drive using outer beams (diamonds) and inner beams (triangles), for CH ablators (blue, green) and Si ablators (orange). Uncertainty in $f_{\rm hot}$ is based on statistical uncertainty in the hard-x-ray data, propagated through EGSnrc modeling.

5 keV. The uncertainty in $f_{\rm hot}$ and $T_{\rm hot}$ are based on the statistical uncertainty in the single-temperature fit to the hard-x-ray spectra. The threshold intensity for the onset of measurable hot electrons in CH targets is approximately 4×10^{14} W/cm^2. This exceeds the calculated absolute SRS threshold ($I_{14}^{\rm SRS,thr} \sim 0.5$) at these conditions, potentially due to a lack of multiple-beam contribution to SRS waves or the presence of convective instabilities.

The inferred hot-electron energy and temperature are consistent with simple arguments based on SRS being their source. From conservation of wave action in the scattering process (i.e., the Manley-Rowe relations [37]), it is determined that, for SRS wavelengths between 600 and 650 nm, the total energy in plasma waves is 0.70 to 0.85 of the total energy in SRS or between 1.4% and 5% of the incident laser energy. Plausibly, kinetic mechanisms such as wave breaking or stochastic processes can convert the plasma-wave energy into hot electrons with an efficiency sufficient to account for the observed quantity ($f_{\rm hot} = 1\%$ to 3%). The characteristic temperature for SRS-generated electrons is often estimated approximately by $T_\phi = \frac{1}{2} m_e v_\phi^2$ [8], where v_ϕ is the phase velocity of the plasma wave. For our experiments, where SRS is observed from wavelengths of ~620 nm to ~702 nm ($2\lambda_0$), the corresponding plasma wave velocities are equivalent to hot-electron temperatures in the range of ~30 to ~85 keV ($T_\phi \sim m_e c^2/6$ for $n_e = n_c/4$). This range of plausible SRS-generated hot-electron temperatures is consistent with the hot electron temperatures that best fit the measured hard-x-ray spectrum.

The combination of $T_{\rm hot}$ and $f_{\rm hot}$ inferred in these experiments is close to the level that can be permitted in direct-drive ignition designs, typically considered to be $f_{\rm hot} \sim 0.5\%$ to 1% for $T_{\rm hot}$ around 50 keV [2,38]. This estimate is based on an allowable coupling of ~0.1% of laser energy to hot-electron preheat in the DT fuel and a near-2π angular divergence of hot electrons inferred in OMEGA spherical experiments [19]. Based on these data, direct-drive ignition designs using a CH ablator and quarter-critical laser intensities of around 5×10^{14} W/cm^2 may be acceptable, but for higher intensities, LPI mitigation is likely to be necessary. The discovery of a regime dominated by SRS, rather than by TPD as on OMEGA, necessitates a reevaluation of the angular divergence of hot electrons at direct-drive ignition-relevant conditions, and may also require reconsideration of mitigation strategies.

One potential LPI mitigation strategy, originally proposed for TPD, uses strategically placed mid-Z layers in the ablator to locally shorten the density scale length, increase the electron temperature, enhance electron-ion collisional damping, and reduce Landau damping of ion-acoustic waves [39–44] to limit the growth of electron plasma waves. This reduction of scale length and increase in temperature are predicted as well for planar Si experiments (L_n from ~690 μm in CH to ~560 μm in Si; T_e from ~4.4 keV in CH to ~5.2 keV in Si), for which hot-electron

data are shown in Fig. 3. The use of Si ablators has a modest effect on hot-electron levels, although it does increase the hot-electron intensity threshold to around 6×10^{14} W/cm^2 based on simulated quarter-critical laser intensities. The lack of hot electrons in this experiment correlates with a minimal level of observed SRS.

In summary, the first experiments to investigate LPI at direct-drive ignition-relevant coronal plasma conditions have revealed evidence of a regime dominated by SRS, including tangential sidescatter. This result is in stark contrast to prior experiments on OMEGA at shorter scale lengths and lower temperatures, in which SRS was minimal and quarter-critical instabilities were identified as TPD. For the first time, intensity thresholds for LPI hot electrons have been evaluated at direct-drive ignition scales, and the use of a Si ablator has been found to have a modest effect, increasing the threshold slightly from $\sim 4 \times 10^{14}$ to $\sim 6 \times 10^{14}$ W/cm^2. These quarter-critical laser intensities present a viable design space for direct drive. As discussed, these results have implications for LPI hot electron preheat mitigation in direct-drive ignition designs, which traditionally have included strategies to mitigate TPD, but will have to consider SRS. Future experiments will characterize the angular distribution of hot electrons, which strongly affects the tolerable level of hot-electron generation and may be different in this SRS-dominated regime than in TPD-dominated experiments on OMEGA [19]. Optical Thomson scattering will ultimately be used on NIF [45,46] to directly probe and characterize plasma waves in the quarter-critical region, as on OMEGA [16], in order to definitively assess the presence or absence of TPD.

The authors thank NIF operations and target fabrication for their assistance in executing these experiments. This material is based upon work supported by the Department of Energy National Nuclear Security Administration under Award No. DE-NA0001944, the University of Rochester, and the New York State Energy Research and Development Authority.

This report was prepared as an account of work sponsored by an agency of the U.S. Government. Neither the U.S. Government nor any agency thereof, nor any of their employees, makes any warranty, express or implied, or assumes any legal liability or responsibility for the accuracy, completeness, or usefulness of any information, apparatus, product, or process disclosed, or represents that its use would not infringe privately owned rights. Reference herein to any specific commercial product, process, or service by trade name, trademark, manufacturer, or otherwise does not necessarily constitute or imply its endorsement, recommendation, or favoring by the U.S. Government or any agency thereof. The views and opinions of authors expressed herein do not necessarily state or reflect those of the U.S. Government or any agency thereof.

*mros@lle.rochester.edu
†Present address: Department of Electrical and Computer Engineering, University of Alberta, Edmonton, Alberta, T6G1H9, Canada.

[1] J. Nuckolls, L. Wood, A. Thiessen, and G. Zimmerman, Nature (London) **239**, 139 (1972).
[2] R. S. Craxton, K. S. Anderson, T. R. Boehly, V. N. Goncharov, D. R. Harding, J. P. Knauer, R. L. McCrory, P. W. McKenty, D. D. Meyerhofer, J. F. Myatt *et al.*, Phys. Plasmas **22**, 110501 (2015).
[3] G. H. Miller, E. I. Moses, and C. R. Wuest, Opt. Eng. **43**, 2841 (2004).
[4] S. Atzeni and J. Meyer-Ter-Vehn, *The Physics of Inertial Fusion: Beam Plasma Interaction, Hydrodynamics, Hot Dense Matter*, International Series of Monographs on Physics (Clarendon, Oxford, 2004).
[5] D. W. Phillion, D. L. Banner, E. M. Campbell, R. E. Turner, and K. G. Estabrook, Phys. Fluids **25**, 1434 (1982).
[6] H. Figueroa, C. Joshi, H. Azechi, N. A. Ebrahim, and K. Estabrook, Phys. Fluids **27**, 1887 (1984).
[7] W. Seka, E. A. Williams, R. S. Craxton, L. M. Goldman, R. W. Short, and K. Tanaka, Phys. Fluids **27**, 2181 (1984).
[8] W. L. Kruer, *The Physics of Laser Plasma Interactions* (Addison-Wesley, Redwood City, CA, 1988).
[9] A. Simon, R. W. Short, E. A. Williams, and T. Dewandre, Phys. Fluids **26**, 3107 (1983).
[10] C. S. Liu, M. N. Rosenbluth, and R. B. White, Phys. Fluids **17**, 1211 (1974).
[11] N. A. Ebrahim, H. A. Baldis, C. Joshi, and R. Benesch, Phys. Rev. Lett. **45**, 1179 (1980).
[12] R. P. Drake, R. E. Turner, B. F. Lasinski, K. G. Estabrook, E. M. Campbell, C. L. Wang, D. W. Phillion, E. A. Williams, and W. L. Kruer, Phys. Rev. Lett. **53**, 1739 (1984).
[13] C. Stoeckl, R. E. Bahr, B. Yaakobi, W. Seka, S. P. Regan, R. S. Craxton, J. A. Delettrez, R. W. Short, J. Myatt, A. V. Maximov, and H. Baldis, Phys. Rev. Lett. **90**, 235002 (2003).
[14] D. T. Michel, A. V. Maximov, R. W. Short, S. X. Hu, J. F. Myatt, W. Seka, A. A. Solodov, B. Yaakobi, and D. H. Froula, Phys. Rev. Lett. **109**, 155007 (2012).
[15] J. F. Myatt, J. Zhang, R. W. Short, A. V. Maximov, W. Seka, D. H. Froula, D. H. Edgell, D. T. Michel, I. V. Igumenshchev, D. E. Hinkel *et al.*, Phys. Plasmas **21**, 055501 (2014).
[16] R. K. Follett, D. H. Edgell, R. J. Henchen, S. X. Hu, J. Katz, D. T. Michel, J. F. Myatt, J. Shaw, and D. H. Froula, Phys. Rev. E **91**, 031104 (2015).
[17] P. Michel, L. Divol, E. L. Dewald, J. L. Milovich, M. Hohenberger, O. S. Jones, L. B. Hopkins, R. L. Berger, W. L. Kruer, and J. D. Moody, Phys. Rev. Lett. **115**, 055003 (2015).
[18] S. Depierreux, C. Neuville, C. Baccou, V. Tassin, M. Casanova, P.-E. Masson-Laborde, N. Borisenko, A. Orekhov, A. Colaitis, A. Debayle *et al.*, Phys. Rev. Lett. **117**, 235002 (2016).
[19] B. Yaakobi, A. A. Solodov, J. F. Myatt, J. A. Delettrez, C. Stoeckl, and D. H. Froula, Phys. Plasmas **20**, 092706 (2013).
[20] J. Lindl, Phys. Plasmas **2**, 3933 (1995).
[21] T. R. Boehly, D. L. Brown, R. S. Craxton, R. L. Keck, J. P. Knauer, J. H. Kelly, T. J. Kessler, S. A. Kumpan, S. J. Loucks, S. A. Letzring *et al.*, Opt. Commun. **133**, 495 (1997).

[22] T. J. B. Collins, J. A. Marozas, K. S. Anderson, R. Betti, R. S. Craxton, J. A. Delettrez, V. N. Goncharov, D. R. Harding, F. J. Marshall, R. L. McCrory *et al.*, Phys. Plasmas **19**, 056308 (2012).
[23] S. Skupsky, R. W. Short, T. Kessler, R. S. Craxton, S. Letzring, and J. M. Soures, J. Appl. Phys. **66**, 3456 (1989).
[24] I. V. Igumenshchev, D. H. Edgell, V. N. Goncharov, J. A. Delettrez, A. V. Maximov, J. F. Myatt, W. Seka, A. Shvydky, S. Skupsky, and C. Stoeckl, Phys. Plasmas **17**, 122708 (2010).
[25] J. D. Moody, P. Datte, K. Krauter, E. Bond, P. A. Michel, S. H. Glenzer, L. Divol, C. Niemann, L. Suter, N. Meezan *et al.*, Rev. Sci. Instrum. **81**, 10D921 (2010).
[26] P. B. Radha, V. N. Goncharov, T. J. B. Collins, J. A. Delettrez, Y. Elbaz, V. Y. Glebov, R. L. Keck, D. E. Keller, J. P. Knauer, J. A. Marozas *et al.*, Phys. Plasmas **12**, 032702 (2005).
[27] W. Seka, B. B. Afeyan, R. Boni, L. M. Goldman, R. W. Short, K. Tanaka, and T. W. Johnston, Phys. Fluids **28**, 2570 (1985).
[28] T. Dewandre, J. R. Albritton, and E. A. Williams, Phys. Fluids **24**, 528 (1981).
[29] The Doppler shift due to plasma flow affects the wavelength of both incoming 351 nm light and outgoing $\omega/2$ light, and constitutes a $\sim$10% effect on the $\omega/2$ wavelength shift. The Dewandre shift results from plasma expansion and an increase in plasma density between the quarter-critical region and the observer as $\omega/2$ propagates outward, and is a $\sim$2% effect on the wavelength shift.
[30] W. Seka, J. F. Myatt, R. W. Short, D. H. Froula, J. Katz, V. N. Goncharov, and I. V. Igumenshchev, Phys. Rev. Lett. **112**, 145001 (2014).
[31] W. Seka, D. H. Edgell, J. F. Myatt, A. V. Maximov, R. W. Short, V. N. Goncharov, and H. A. Baldis, Phys. Plasmas **16**, 052701 (2009).
[32] S. Weber and C. Riconda, High Power Laser Sci. Eng. **3**, e6 (2015).
[33] B. B. Afeyan and E. A. Williams, Phys. Fluids **28**, 3397 (1985).
[34] R. P. Drake, R. E. Turner, B. F. Lasinski, E. A. Williams, K. Estabrook, W. L. Kruer, E. M. Campbell, and T. W. Johnston, Phys. Rev. A **40**, 3219 (1989).
[35] M. Hohenberger, F. Albert, N. E. Palmer, J. J. Lee, T. Dppner, L. Divol, E. L. Dewald, B. Bachmann, A. G. MacPhee, G. LaCaille *et al.*, Rev. Sci. Instrum. **85**, 11D501 (2014).
[36] I. Kawrakow, Med. Phys. **27**, 485 (2000).
[37] J. M. Manley and H. E. Rowe, Proc. IRE **44**, 904 (1956).
[38] M. Hohenberger, P. B. Radha, J. F. Myatt, S. LePape, J. A. Marozas, F. J. Marshall, D. T. Michel, S. P. Regan, W. Seka, A. Shvydky *et al.*, Phys. Plasmas **22**, 056308 (2015).
[39] R. E. Turner, K. Estabrook, R. L. Kauffman, D. R. Bach, R. P. Drake, D. W. Phillion, B. F. Lasinski, E. M. Campbell, W. L. Kruer, and E. A. Williams, Phys. Rev. Lett. **54**, 189 (1985).
[40] V. A. Smalyuk, R. Betti, J. A. Delettrez, V. Y. Glebov, D. D. Meyerhofer, P. B. Radha, S. P. Regan, T. C. Sangster, J. Sanz, W. Seka *et al.*, Phys. Rev. Lett. **104**, 165002 (2010).
[41] J. F. Myatt, H. X. Vu, D. F. DuBois, D. A. Russell, J. Zhang, R. W. Short, and A. V. Maximov, Phys. Plasmas **20**, 052705 (2013).
[42] S. X. Hu, D. T. Michel, D. H. Edgell, D. H. Froula, R. K. Follett, V. N. Goncharov, J. F. Myatt, S. Skupsky, and B. Yaakobi, Phys. Plasmas **20**, 032704 (2013).
[43] R. K. Follett, J. A. Delettrez, D. H. Edgell, V. N. Goncharov, R. J. Henchen, J. Katz, D. T. Michel, J. F. Myatt, J. Shaw, A. A. Solodov, C. Stoeckl, B. Yaakobi, and D. H. Froula, Phys. Rev. Lett. **116**, 155002 (2016).
[44] J. R. Fein, J. P. Holloway, M. R. Trantham, P. A. Keiter, D. H. Edgell, D. H. Froula, D. Haberberger, Y. Frank, M. Fraenkel, E. Raicher *et al.*, Phys. Plasmas **24**, 032707 (2017).
[45] P. Datte, J. Ross, D. Froula, J. Galbraith, S. Glenzer, B. Hatch, J. Kilkenny, O. Landen, A. Manuel, W. Molander *et al.*, J. Phys. Conf. Ser. **717**, 012089 (2016).
[46] J. S. Ross, P. Datte, L. Divol, J. Galbraith, D. H. Froula, S. H. Glenzer, B. Hatch, J. Katz, J. Kilkenny, O. Landen *et al.*, Rev. Sci. Instrum. **87**, 11E510 (2016).